OPEN ACCESS
PAPER

Mongolian Journal of Geography and Geoecology - MJGG

Received: 09 May 2025; Accepted: 23 June 2025; Published online: 1 September 2025
https://doi.org/10.5564/mjgg.v62i46.4126

Topoclimatic drivers of land cover change in the Mongol Altai Mountains using random forest and eXtreme gradient boosting algorithms

***CORRESPONDING AUTHOR**
Batnyam Tseveengerel
batnyamts@mas.ac.mn
ORCID
0000-0002-9634-5243

CITATION
Batnyam Ts, Purevsuren M, Renchinmyadag T (2025) Topoclimatic Drivers of Land Cover Change in The Mongol Altai Mountains Using Random Forest and eXtreme Gradient Boosting Algorithms.
Mongolian Journal of Geograhy and Geoecology, 62(46), 1–11.
https://doi.org/10.5564/mjgg.v62i46.4126

Batnyam Tseveengerel[1,*], Purevsuren Munkhtur[1], Renchinmyadag Tovuudorj[1]

[1]*Institute of Geography and Geoecology, Mongolian Academy of Sciences, Ulaanbaatar 15170, Mongolia*

ABSTRACT
Investigating land cover change in mountainous regions is crucial for sustainable land use planning and enhancing climate adaptation strategies. This study examines the spatial and temporal patterns of land cover dynamics in the Mongol Altai Mountains over a 30-year period, and identifies the key climatic and topographic factors, collectively referred topoclimatic drivers, that influencing these changes. Landsat satellite imagery with a 30 m resolution was processed using the Random Forest (RF) algorithm in R to classify land cover types. A change detection matrix was employed to quantify transitions between land cover types, and the results were visualized using a Sankey diagram. To assess the impact of environmental variables, eXtreme Gradient Boosting (XGBoost) algorithm was applied and model interpretability was enhanced using SHAP (Shapley Additive exPlanations) values. The classification demonstrated high accuracy, with overall accuracy values of 92.5% for 1990 and 93.7% for 2020. Over the study period, notable declines were observed in grasslands (−20.08%), tree-covered areas (−22.84%), and glaciers (−43.01%), while shrublands (26.82%) and artificial surfaces (36.28%) experienced substantial increases. XGBoost analysis identified vapor pressure, elevation, and wind speed as the most significant environmental factors driving land cover change. These factors demonstrated complex, non-linear relationships, highlighting the heterogeneous nature of high mountain ecosystems. The findings provide valuable insights for formulating climate-responsive land management and conservation strategies in mountainous regions.

KEYWORDS
Mongol Altai Mountains, Land cover change, Random forest, XGBoost, SHAP, Topoclimatic drivers, Climatic variables

1. INTRODUCTION

Land use and land cover change (LULC) represents a fundamental process linked to global environmental change, influencing both local and global ecosystems [1]. Cimate change has exacerbated desertification and land degradation, particularly in the middle and high latitudes of the northern hemisphere [2]. Mountainous regions, which are highly diverse in terms of geography, shape, altitude, vegetation, and climate, experiences the impacts of climate change in unique ways. Therefore, findings from one mountainous region cannot be directly applied to others due to these differences [3], [4]. Thus, this variability limits the applicability of regional research outcomes to other mountainous areas.

The Altai Mountains, located in Central Asia, are important both ecologically and climatologically [5], [6]. In recent years, Mongolia has experienced substantial environmental and resource use changes, largely driven by rapid climate change [7], [8], [9]. While significant studies on land cover and land use change have been conducted at the national level and Mongolian Plateau, such as the research by Yu Zhang et al. [10] on the land cover changes in the Mongolian Plateau, Juanle Wang et al. [11] on land cover changes from 1990 to 2010, and Junming et al. [12] on land cover changes in Mongolia from 1990 to 2021, and its drivers . In addition, numerous studies have been conducted at the regional and local levels on land cover and land use changes, as well as the factors influencing these changes [13], [14], [15], [16], [17], [18], [19], [20].

Nevertheless, there remains a gap in the understanding of how these changes are influenced by climatic and topographic factors in mountainous regions. High mountain regions are particularly important for land cover change studies due to their sharp topographic gradients and climatic heterogeneity, which together create complex and spatially variable ecosystem responses [21], [22]. These areas are highly sensitive to elevation-dependent warming, influencing vegetation zones, snow cover, and hydrological regimes. As a result, the combined effects of climatic and topographic drivers are amplified, exerting a significant influence on land cover dynamics [23], [24].

The aim of this study is to investigate the pattems of land cover change in the Mongol Altai Mountains and explore the relationship between land cover changes with climatic and topographic variables. The findings from this research are expected to enhance the understanding of the spatial dynamics of land cover in mountainous regions and contribute to the development of sustainable land management and climate adaptation strategies for Mongolia's highland ecosystems.

2. STUDY AREA, DATA AND METHODS

2.1 Study area

The Altai Mountain Range extends approximately 2,100 kilometers across China, Mongolia, Russia, and Kazakhstan [25]. Within this range, the Mongol Altai Mountainous area stretches roughly 800 kilometers from Tavan Bogd Mountain in the northwest to the depression of Alag Lake in the southeast [26].

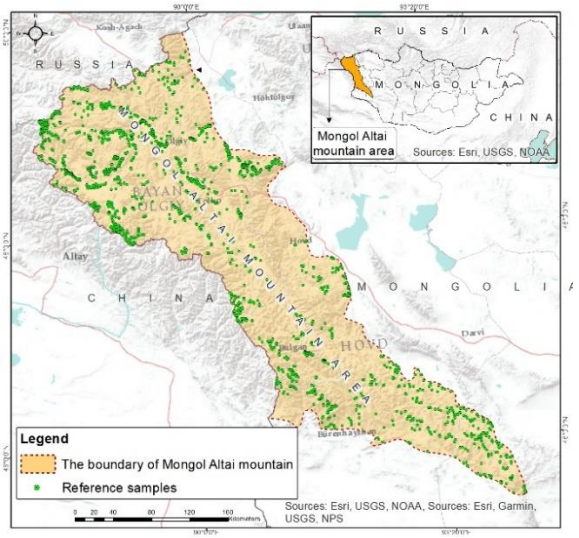

Figure 1. Study area and reference samples

This study focuses specifically on the Mongol Altai Mountains as the study area. The region spans a total area of 69376.6 km^2, with elevations ranging from 1210 to 4374 m above sea level, reflecting significant topographic variability.

2.2 Materials

Satellite data

Medium-resolution (30 m) Landsat satellite imagery was used for land cover classification and analysis. The datasets were sourced from NASA Earthdata [27] and accessed on 5 April 2025.

Table 1. Satellite data

Satellite	Band used	Year
Landsat 5 TM	Bands 1-5, 7	1988-2022
Landsat 8 OLI	Band 2-7	2018-2022
Landsat 9 OLI-2	Band 2-7	2021-2022

Given the extensive and mountainous relief of the study area, image selection was carefully adjusted to minimize cloud cover and ensure high-quality visual data. As such, imagery was chosen from within a one or two year range of the target dates, and in some cases, images from up to ±4 years were used to compensate for limited cloud-free observations. To ensure seasonal consistency, only summer images (June to August) were selected, thereby minimizing phenological variation and ensuring comparability across years. In addition to the satellite imagery, surface elevation data were derived from the Advanced Spaceborne Thermal Emission and Reflection Radiometer (ASTER) Global Digital Elevation Model (GDEM) with a spatial resolution of 30 meters [28].

Climate data

To characterize the climatic conditions of the study area, several high-resolution monthly climate variables were obtained from the TerraClimate dataset [29]. The selected variables included minimum air temperature (Tmin), maximum air temperature (Tmax), precipitation, wind speed, and vapor pressure (i.e., the partial pressure of water vapor in air). TerraClimate provides data at an approximate spatial resolution of 4 km (~1/24°), derived from a combination of ground-based meteorological observations and climate reanalysis products [29]. The climate data were downloaded in NetCDF format from the TerraClimate repository, maintained by the Climatology Lab at the University of California, Merced [29].

The variables were processed using R and ArcGIS software to generate spatial layers that corresponded with the acquisition periods of the Landsat imagery, used in the analysis.

2.3 Data Pre-Processing

Atmospheric and radiometric corrections were performed on Landsat 5 TM, Landsat 8 OLI, and Landsat 9 OLI-2 imagery to reduce atmospheric distortions and ensure cross-sensor consistency. To enhance the spectral separability of land cover classes and improve classification accuracy, a set of spectral indices related to vegetation, water, built-up areas, and snow cover were estimated (Table 2).

Each index was estimated using the spectral bands specific to each satellite sensor. In addition, topographic variables such as slope and elevation were derived from the ASTER GDEM dataset with a spatial resolution of 30 m.

Table 2. Overview of key remote sensing indices and topographic variables used in the land cover classification

Sources	Variables	Formula, Reference
Landsat 5 TM, Landsat 8 OLI, Landsat 9 OLI-2	NDVI	(NIR – Red) / (NIR + Red), [30]
	EVI	G × (NIR – Red) / (NIR + C1 × Red – C2 × Blue + L), [31]
	SAVI	((NIR – Red) / (NIR + Red + L)) × (1 + L), [32]
	OSAVI	(NIR – Red) / (NIR + Red + 0.16), [33]
	DVI	NIR – Red, [34]
	MNDWI	(Green – SWIR1) / (Green + SWIR1), [35]
	NDBI	(SWIR – NIR) / (SWIR + NIR), [36]
	NDSI	(Green – SWIR) / (Green + SWIR), [37]
Aster DEM	Slope	Steepness
	Elevation	Distance above sea level

Abbreviations: NDVI (Normalized Difference Vegetation Index), EVI (Enhanced Vegetation Index), SAVI (Soil Adjusted Vegetation Index), OSAVI (Optimized Soil Adjusted Vegetation Index), DVI (Difference Vegetation Index), MNDWI (Modified Normalized Difference Water Index), NDBI (Normalized Difference Built-up Index), NDSI (Normalized Difference Snow Index), DEM (Digital Elevation Model), TWI (Topographic Wetness Index), TPI (Topographic Position Index).

2.4 Training and Validation Sample Preparation

In this study, a total of 2200 reference samples were generated through visual interpretation of Landsat imagery, supplemented by auxiliary data (Figure 1). To facilitate model development and assessment, the samples were randomly divided using the R programming language, with 70% (1540 points) allocated for training and 30% (660 points) for validation. A stratified random sampling approach [38], [39] was employed to ensure proportional representation of all land cover classes, thereby enhancing the robustness and reliability of the classification process.

2.5 Land cover classification and land cover change

RF algorithm is widely recognized for its robustness and accuracy in land cover classification, particularly due to its capacity to handle high-dimensional data, reduce overfitting, and provide reliable classification results [23]. In this study, land cover in the Mongol Altai Mountains was classified for the years 1990 and 2020 using the RF algorithm implemented in the R programming environment via the *randomForest* package. Input variables included Landsat spectral bands, derived spectral indices and

topographic variables such as elevation and slope (Table 2).

Land cover was classified based on the Food and Agriculture Organization's Land Cover Classification System (LCCS) and the Land Cover Meta Language (LCML) framework (FAO, 2010). The classified categories followed the LCML framework (FAO, 2010) were coded accordingly: grassland (A23), tree-covered area (A11), shrubs and herbaceous vegetation (A12/A22), sparsely naturally vegetated area (B1), terrestrial barren land (D1), permanent snow and glaciers (E2), and inland water bodies (F1). Due to spectral confusion between built-up areas and other classes, built-up areas (C-1) were manually digitized using ArcGIS for ensuring reliable classification using spectral indices.

To quantify the intensity and direction of land cover change over the study period, we employed a comprehensive land cover change degree model based on a transition matrix approach. This model captures the aggregated extent of land cover conversions between classes and expresses the result as a percentage per year, allowing for consistent comparison across time intervals. The formula used is as follows [40]:

$$LC = \left[\frac{\sum_{i=1}^{n}\sum_{j=1}^{n}|\Delta LU_{i-j}|}{2\sum_{i=1}^{n}\Delta LU_i}\right] \times \frac{1}{T} \times 100\% \quad (1)$$

Where, ΔLU_{i-j} is the area converted from land cover type i to type j, ΔLU_i -is the total change area of type i, n-is the total number of land cover categories, T- is the study period, which is 30 years, LC - represents the annual intensity of land cover change.

2.6 Accuracy assessment

Classification performance was assessed using standard accuracy metrics derived from the confusion matrix. These included Overall Accuracy (OA), the Kappa coefficient, and the 95% Confidence Interval (CI) for OA. OA quantifies the proportion of correctly classified samples among all validation points out of the total, while the Kappa coefficient provides a measure of agreement adjusted for the agreement that might occur by chance, offering a more statistically rigorous assessment of model performance.

To further assess classification reliability, the Accuracy Lower and Accuracy Upper bounds of the 95% confidence interval were calculated. The Accuracy Null metric estimates the accuracy of a random classifier, and the Accuracy p-Value tests whether the model significantly outperforms random classification. All accuracy statistics were computed using the confusion Matrix function from the caret package in R [41]. The relevant equations are as follows:

$$OA = \frac{\sum_{i=1}^{k} n_{ii}}{N} \quad (2)$$

Where, n_{ii}-Number of correctly classified samples in class i, N- total number of validation samples, k- total number of classes

$$k = \frac{P_o - P_e}{1 - P_e} \quad (3)$$

Where, P_o -Observed agreement, P_e -expected agreement.

$$CI_{95\%} = OA \pm z \cdot \sqrt{\frac{OA(1-OA)}{N}} \quad (4)$$

Where, z - 1.96 (for 95% confidence level), N - Number of validation samples;

2.7 Analysis of Driving Factor

A variety of statistical and machine learning approaches, including logistic regression, support vector machines, random forests, and gradient boosting methods, have been employed to assess the influence of environmental variables on land cover change [42], [43] Among these, eXtreme Gradient Boosting (XGBoost) has demonstrated superior predictive performance and computational efficiency, particularly in modeling complex, non-linear relationships and variable interactions [44]. Therefore, in this study, the XGBoost algorithm was applied to evaluate the influence of climatic and topographic variables on land cover change between 1990 and 2020.

Table 3. Explanatory variables used in the XGBoost model and their data sources.

№	Variable Name	Data Source
1	Elevation (DEM)	ASTER GDEM
2	Slope	Calculated from ASTER GDEM
3	Aspect	
4	Topographic Position Index (TPI)	
5	Topographic Wetness Index (TWI)	
6	Mean Temperature (tmean)	TerraClimate
7	Maximum Temperature (tmax)	TerraClimate
8	Minimum Temperature (tmin)	TerraClimate
9	Precipitation (ppt)	TerraClimate
10	Wind Speed (ws_mean)	TerraClimate
11	Vapour Pressure (vap_mean)	TerraClimate

A total of explanatory variables, including both topographic and climatic factors, were used in the XGBoost model. These variables, along with their data sources, are listed in Table 3. All variables were selected based on relevance to land cover dynamics

and availability of consistent spatial data over the study area.

The model was trained using the XGboost package in R with a binary logistic objective (binary:logistic), a maximum tree depth of 6, and 100 boosting iterations. To interpret the relative contribution of each variable, SHapley Additive exPlanations (SHAP) values were calculated. SHAP provides a unified framework for interpreting model outputs by quantifying the marginal contribution of each feature to individual predictions, thus enabling both global and local interpretability. The influence of environmental drivers was further examined using SHAP summary and dependence plots, which visualized feature importance and interaction effects, respectively.

3. RESULT AND DISCUSSION

3.1 Overview of Classification Results

An analysis of land cover change in the Mongol Altai Mountains over the past 30 years (1990–2020) revealed pronounced shifts in land cover classes at the total area of the study area (**Figure 2**). The most notable expansion was observed in sparsely natural vegetated areas (LC4), which increased by 12.2%. In contrast, grasslands (LC2) exhibited the most substantial reduction, declining by 5.9%.

Additionally, terrestrial barren land (LC5) also showed a marked decrease of 5.7%, while moderate reductions were recorded in tree-covered areas (LC1) and permanent snow and glaciers (LC6), both of which declined by 0.6%. Inland water bodies (LC7) experienced a slight decrease of 0.2%. Meanwhile, shrubs and herbaceous vegetation (LC3) demonstrated a minor increase of 0.7%.

When comparing the area changes for 3 decades only within the specific land cover classes (Figure 3), the most significant increase was recorded in artificial surfaces (LC8), which expanded by 36.28%, followed by shrubs and herbaceous vegetation (LC3) with a 26.82% increase, and LC4, which grew by 26.60%. On the other hand, the substantial decline was observed LC5, which contracted by 49.94%. This was accompanied by major losses in permanent snow and glaciers (LC6) (−43.01%), LC1 (−22.84%), LC7 (−21.66%), and LC2 (−20.08%). These results, categorized under LC1 to LC8, reveal substantial spatial shifts in land cover composition, reflecting the cumulative effects of climatic and terrain-related drivers across the region.

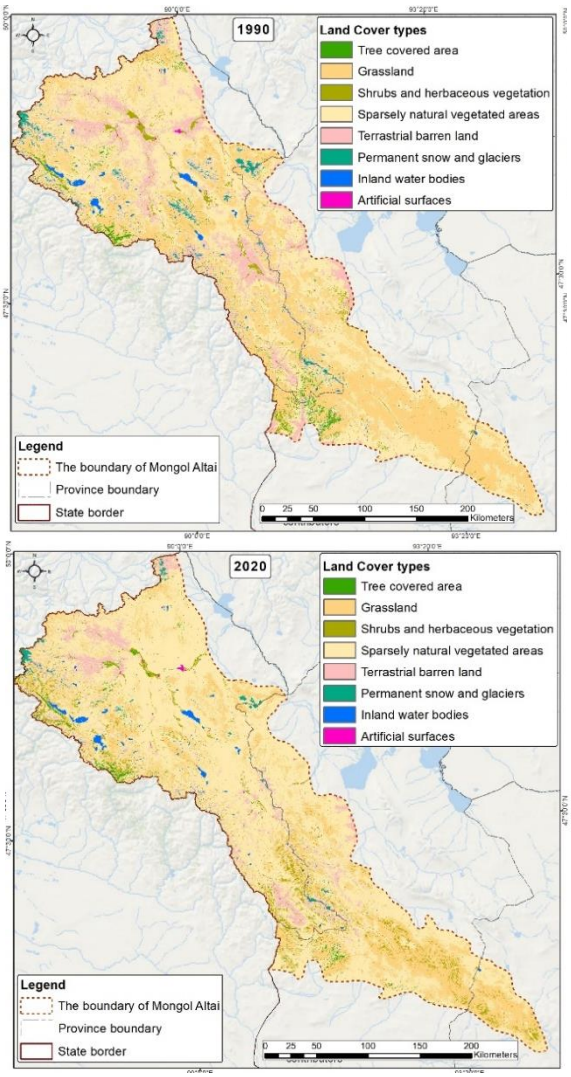

Figure 2. Land cover changes from 1990 to 2020

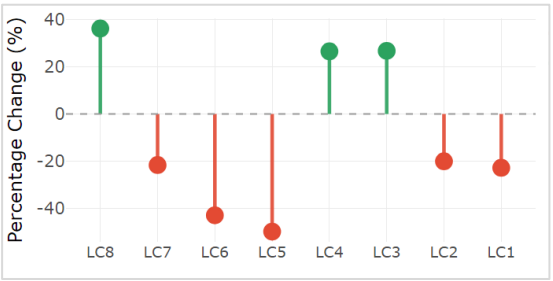

Figure 3. Area change for each land cover class

3.2 Land Cover Transition Matrix and Sankey Diagram Interpretation

To visualize the magnitude and direction of land cover changes, a land cover transition matrix was first constructed. This matrix quantifies the extent to which land shifted from one category to another over the study period, offering a detailed representation of

inter-class transitions. To enhance interpretability, the transition data were further visualized using a Sankey diagram generated in R via the networkD3 package. In this diagram, the width of each stream represents the area of land that transitioned from a specific land cover class in 1990 to a different class in 2020.

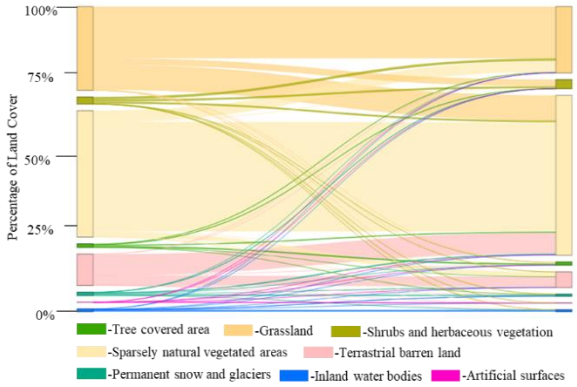

Figure 4. Sankey diagram of land cover changes from 1990 to 2020

Several notable transition patterns emerged from the analysis. These included the conversion of LC2 to LC4, indicating a shift potentially driven by land degradation processes. Likewise, LC6 showed significant retreat, with many areas transitioning into LC5 and LC4. These changes are indicative of broader climatic shifts, including glacial melting. Additionally, a considerable fraction of LC5 was transformed into LC3, as well as into LC8, reflecting ongoing land use modifications (**Figure 4**).

3.3 SHAP-Based Interpretation of Land Cover Change Drivers

To gain a more detailed understanding of how each environmental variable influences land cover change, we employed both the SHAP summary plot (Figure 5) and a series of SHAP dependence plots (Figure 6). These visualizations provide insight not only into the average importance of each driver but also into the functional relationships between variable values and their contributions to model predictions by capturing nonlinear, threshold-based effects.

As shown in Figure 5, vapor pressure (vap) was identified as the most influential variable, with a mean a SHAP value of 0.256. It was followed by elevation (DEM) with a SHAP value of 0.217, and wind speed (ws) at 0.197. High vapor pressure values (represented in purple on the plot) were associated with positive SHAP values, indicating that increased atmospheric moisture enhances the probability of land cover change. This may be attributed to improved vegetation productivity or climate-facilitated transitions.

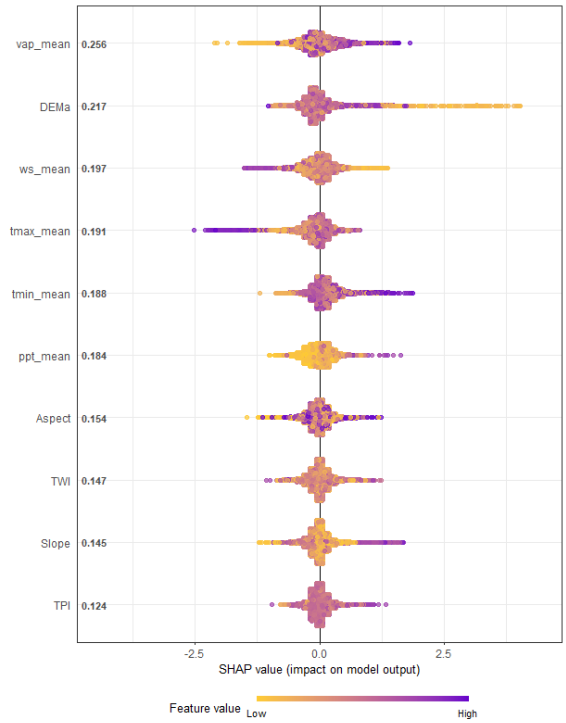

Figure 5. SHAP summary plot

In Figure 6, Elevation (DEMa) showed a strong threshold pattern: SHAP values increased with elevation up to a mid-altitudinal range, after which their influence gradually diminished. This trend reflects the ecological zonation of mountainous regions, where mid-elevation zones are often more dynamic in terms of vegetation productivity and land cover transitions [45].

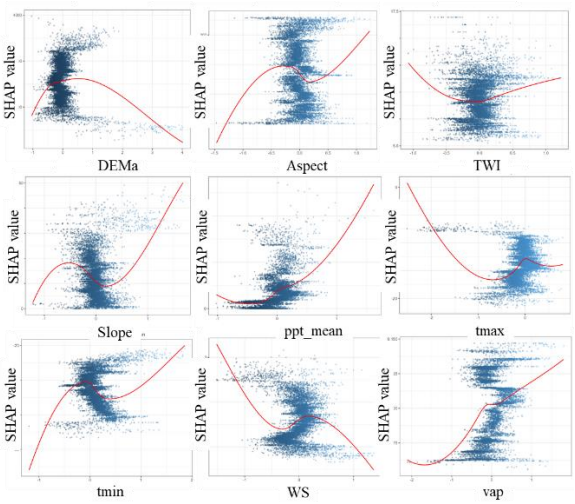

Figure 6. SHAP summary plot showing the relative importance of predictor variables in the XGBoost

model. Variables include elevation (DEMa), topographic wetness index (TWI), slope, aspect, maximum temperature (tmax), minimum temperature (tmin), precipitation (ppt_mean), wind speed (WS), and vapour pressure (vap)

Precipitation (ppt_mean) showed a sharp increase in SHAP values from moderate to high levels, indicating that transitional land cover is more likely to occur in areas with moderate rainfall availability.

Both maximum (tmax) and minimum temperature (tmin) exhibited inflection points, reflecting nonlinear effects of thermal conditions on land cover change. Extremely low temperatures were associated with negative SHAP values, indicating a suppressive influence on vegetation dynamics, particularly in high-altitude or permafrost-affected areas. Conversely, moderate warming corresponded with increasingly positive SHAP values, suggesting that rising temperatures may promote vegetation expansion and changes in surface cover. This pattern is consistent with findings from the Russian Far East, where Wang et al. [46] reported that thermal regimes significantly influenced land use and cover changes, especially under warming trends that enhanced vegetation activity.

Topographic variables such as slope, TWI, and aspect showed curvilinear relationships with land cover change. Moderate slopes contributed more positively, likely due to balanced drainage and moisture conditions, while steep and flat terrains had lower influence. Steep slopes limit vegetation through erosion and runoff, whereas flat areas may retain excess water and restrict plant diversity. These results support findings by Wang et al. [47], who highlighted the significance of terrain features in influencing land cover dynamics in complex landscapes.

3.4 Ecological implications

The substantial reduction in grasslands (−20.08%), forests (−22.84%), and glaciers (−43.01%) across the Mongolian Altai reflects reduced ecosystem productivity and increased vulnerability to soil erosion and hydrological imbalance. These changes align with regional glacial retreat trends [48] and highlight potential losses in ecosystem services such as carbon storage and moisture retention [49]. SHAP results suggest that climatic factors, particularly vapor pressure and wind speed, and terrain characteristics play critical roles. The observed shift toward shrubland may represent both climate adaptation and early-stage desertification [50].

3.5 Regional Context

In contrast to relatively stable land cover dynamic reported in central and eastern Mongolia [51], [52], the Mongol Altai region shows pronounced ecological transformation. This accelerated change is consistent with findings from global alpine regions, which demonstrate heightened sensitivity to climatic warming and environmental stressors [52]. The substantial expansion of artificial surfaces (36.28%) and shrubland (26.82%) likely reflects intensifying land use pressures, shifts in vegetation patterns, and broader ecological responses to both anthropogenic and climatic influences. These transitions contribute to increased landscape fragmentation, with potential implications for biodiversity, habitat connectivity, and regional ecological stability.

3.6 Accuracy and Evaluation

RF model showed strong classification performance for both 1990 and 2020 land cover maps. In 1990, the overall accuracy was 92.5% with a Kappa coefficient of 0.91, and a 95% confidence interval ranging from 91.31% to 95.74%. For 2020, accuracy improved slightly to 93.7%, with a Kappa coefficient of 0.915 and a confidence interval of 91.25%–95.73%. The null accuracy remained low in both years (17.15% and 17.42%, respectively), confirming the model's reliability. These results suggest that the RF algorithm offers a dependable framework for long-term land cover change detection, with minimal classification error and high statistical confidence.

4. CONCLUSION

This study investigated the spatial and temporal dynamics of land cover change in the Mongol Altai Mountains over the past 30 years (1990–2020), and identified the main climatic and topographic drivers influencing these transformations. The analysis revealed a significant decline in ecologically critical land cover classes: grasslands (−20.08%), tree-covered areas (−22.84%), and glaciers (−43.01%) coupled with marked expansions in shrublands (26.82%) and artificial surfaces (36.28%). These shifts indicate significant alterations in the composition and structure of the alpine ecosystem, likely driven by both anthropogenic pressures and climate-induced processes.

The classification accuracy exceeded 92% in both years, confirming the reliability of the Random Forest algorithm. More importantly, SHAP-based interpretation of the XGBoost model provided new insights into the complex interactions between

topographic and climatic variables. Vapor pressure, elevation, and wind speed emerged as the most influential drivers, each showing nonlinear and threshold effects. For instance, mid-elevation ranges (2200–2800 m) exhibited the highest land cover transition probabilities, likely due to greater vegetation sensitivity and accessibility. Increased vapor pressure promoted vegetation growth or succession, while higher wind speed contributed to ecological instability.

By integrating SHAP into the modeling framework, this study achieved high predictive performance and improved interpretability, bridging the methodological gap between data-driven modeling and ecological reasoning. This approach illustrates the potential of interpretable artificial intelligence to inform climate-adaptive land management and conservation planning.

In conclusion, the Mongol Altai Mountains are undergoing pronounced and complex land cover transitions, driven by climatic and topographic variability. The results emphasize the critical need for elevation-sensitive conservation planning and highlight the utility of interpretable machine learning models in high-altitude environmental research. Moreover, future research should explore higher spatial resolution analysis and include additional biophysical and ecological indicators for further refining our understanding of land cover dynamics in mountainous ecosystems under accelerating environmental change.

ACKNOWLEDGMENTS

The authors would like to thank all colleagues at the Division of Physical Geography, Institute of Geography and Geoecology, Mongolian Academy of Sciences, for their valuable support and assistance throughout this study.

REFERENCES

[1] J. A. Foley, et al., “Global consequences of land use,” *Science (1979)*, vol. 309, no. 5734, pp. 570–574, 2005. Available: doi: 10.1126/science.1111772

[2] T. Stoerk, G. Wagner, and R. E. T. Ward, “Policy brief—Recommendations for improving the treatment of risk and uncertainty in economic estimates of climate impacts in the sixth Intergovernmental Panel on Climate Change assessment report,” *Rev Environ Econ Policy*, 2018. Available: doi: 10.1093/reep/rey005

[3] T. Kohler and D. Maselli, “Mountains and climate change,” From understanding to action. Geographica Bernensia, 2009.

[4] B. Hewitson, et al., “Regional context,” in Climate change 2014: Impacts, adaptation and vulnerability: Part B: Regional aspects: Working Group II Contribution to the Fifth Assessment Report of the Intergovernmental Panel on Climate Change, Cambridge University Press, 2015, pp. 1133–1198.

[5] X. Chen, “Physical Geography of China’s Arid Zones,” 2010, Beijing: Science Press (in Chinese).

[6] E. M. Aizen, V. B. Aizen, J. M. Melack, T. Nakamura, and T. Ohta, “ Precipitation and atmospheric circulation patterns at mid - latitudes of Asia," *Int J Climatol*, vol. 21, no. 5, pp. 535 – 556, 2001. Available: doi: 10.1002/joc.626

[7] J. Tsogtbaatar, S. Khudulmur, N. Mandakh, and S. Amartuvshin, “A Spatial and Temporal Assessment of Forest Cover Changes in Mongolia Using Remotely Sensed Data,” in Salt Lake city, USA, IUFRO 2014 congress, Institute of Geoecology, 2014.

[8] S. Vandandorj, E. Munkhjargal, B. Boldgiv, and B. Gantsetseg, “Changes in event number and duration of rain types over Mongolia from 1981 to 2014,” *Environ Earth Sci,* vol. 76, no. 2, p. 70, 2017. Available: doi: 10.1007/s12665-016-6380-0

[9] R. Törnqvist, et al., “Evolution of the hydro-climate system in the Lake Baikal basin,” *J Hydrol (Amst),* vol. 519, pp. 1953–1962, 2014. Available: doi: 10.1016/j.jhydrol.2014.09.074

[10] Y. Zhang, J. Wang, Y. Wang, A. Ochir, and C. Togtokh, “Land Cover Change Analysis to Assess Sustainability of Development in the Mongolian Plateau over 30 Years,” *Sustainability (Switzerland),* vol. 14, no. 10, May 2022, Available: doi: 10.3390/su14106129.

[11] J. Wang, “Land cover patterns in Mongolia and their spatiotemporal changes from 1990 to 2010,” *Arab J Geosci,* p. 13, 2019, [Online]. Available: files/202/Wang - 2019 - Land cover

patterns in Mongolia and their spatiote.pdf. Available: doi: 10.1007/s12517-019-4893-z

[12] J. Hao et al., "Spatial–Temporal and Driving Factors of Land Use/Cover Change in Mongolia from 1990 to 2021," *Remote Sens (Basel),* vol. 15, no. 7, Apr. 2023, Available: doi: 10.3390/rs15071813.

[13] J. Yuan et al., "Land Use Hotspots of the Two Largest Landlocked Countries: Kazakhstan and Mongolia," *Remote Sens (Basel),* vol. 14, no. 8, Apr. 2022, Available: doi: 10.3390/rs14081805.

[14] C. Sun, Y. Bao, B. Vandansambuu, and Y. Bao, "Simulation and Prediction of Land Use/Cover Changes Based on CLUE-S and CA-Markov Models: A Case Study of a Typical Pastoral Area in Mongolia," *Sustainability (Switzerland)*, vol. 14, no. 23, Dec. 2022, Available: doi: 10.3390/su142315707.

[15] S. Dong, Y. Li, Y. Li, and S. Li, "Spatiotemporal patterns and drivers of land use and land cover change in the china-mongolia-russia economic corridor," *Pol J Environ Stud*, vol. 30, no. 3, pp. 2527–2541, 2021, Available: doi: 10.15244/pjoes/127419.

[16] N. Dugarsuren, C. Lin, and K. Tsogt, "Land cover change detection in Mongolia in last decade using MODIS imagery," *Proc. Asian Conf. Remote Sens. (ACRS)*, Taipei, Taiwan, p. 688, 2011.

[17] J. Yuan and J. Chen, "Disproportionate contributions of land cover and changes to ecosystem functions in Kazakhstan and Mongolia," *Sci Rep,* vol. 14, no. 1, p. 21922, Dec. 2024, Available: doi: 10.1038/s41598-024-72231-3.

[18] M. Lamchin, et al., "Assessment of land cover change and desertification using remote sensing technology in a local region of Mongolia," *Advances in Space Research, vol*. 57, no. 1, pp. 64–77, Jan. 2016, Available: doi: 10.1016/j.asr.2015.10.006.

[19] J. A. Priess, C. Schweitzer, F. Wimmer, O. Batkhishig, and M. Mimler, "The consequences of land-use change and water demands in Central Mongolia," *Land use policy,* vol. 28, no. 1, pp. 4–10, Jan. 2011, Available: doi: 10.1016/j.landusepol.2010.03.002.

[20] B. Vandansambuu, T. Davaa, B. Gantumur, M. Purevtseren, O. Lkhagva, and F. Wu, "Spatiotemporal monitoring and prediction of land use/land cover changes using CA-Markov chain model: a case study in Orkhon Province, Mongolia," *SPIE-Intl Soc Optical Eng,* Sep. 2020, p. 12. Available: doi: 10.1117/12.2574032.

[21] C. Körner, J. Paulsen, and E. M. Spehn, "A definition of mountains and their bioclimatic belts for global comparisons of biodiversity data," *Alp Bot,* vol. 121, no. 2, pp. 73–78, 2011, Available: doi: 10.1007/s00035-011-0094-4.

[22] D. Scherrer and C. Körner, "Topographically controlled thermal-habitat differentiation buffers alpine plant diversity against climate warming," *J Biogeogr,* vol. 38, no. 2, pp. 406–416, 2011, Available: doi: 10.1111/j.1365-2699.2010.02407.x.

[23] N. Pepin, et al., "Elevation-dependent warming in mountain regions of the world," *Nat Clim Chang*, vol. 5, no. 5, pp. 424–430, 2015, Available: doi: 10.1038/nclimate2563.

[24] E. Palazzi, L. Filippi, and J. Von Hardenberg, "Insights into elevation-dependent warming in the Tibetan Plateau–Himalayas from CMIP5 model simulations," *Clim Dyn,* vol. 52, pp. 5833–5849, 2019, Available: doi: 10.1007/s00382-018-4485-6.

[25] G. Chen et al., "Natural world heritage sites are at risk from climate change globally," *Commun Earth Environ,* vol. 5, no. 1, 2024. Available: doi: 10.1038/s43247-024-01933-3

[26] S.Jigj, Fundamental Features of the Relief of Mongolia. Ulaanbaatar: Publishing House of the Academy of Sciences, 1975.

[27] NASA, "Earthdata: Data from NASA's Earth science missions."

[28] NASA/METI/AIST/Japan Spacesystems and U.S./Japan ASTER Science Team, "ASTER Global Digital Elevation Model V003," NASA EOSDIS Land Processes DAAC.

[29] J. T. Abatzoglou, S. Z. Dobrowski, S. A. Parks, and K. C. Hegewisch, "TerraClimate, a high-resolution global dataset of monthly climate and climatic water balance from 1958–2015," *Sci Data,* vol. 5, no. 1, pp. 1–12, 2018. Available: doi: 10.1038/sdata.2017.191

[30] C. J. Tucker, "Red and photographic infrared linear combinations for monitoring vegetation,"

Remote Sens Environ, vol. 8, no. 2, pp. 127–150, 1979. Available: doi: 10.1016/0034-4257(79)90013-0

[31] A. Huete, K. Didan, T. Miura, E. P. Rodriguez, X. Gao, and L. G. Ferreira, "Overview of the radiometric and biophysical performance of the MODIS vegetation indices," *Remote Sens Environ,* vol. 83, no. 1–2, pp. 195–213, 2002. Available: doi: 10.1016/S0034-4257(02)00096-2

[32] A. R. Huete, "A soil-adjusted vegetation index (SAVI)," *Remote Sens Environ,* vol. 25, no. 3, pp. 295–309, 1988. Available: doi: 10.1016/0034-4257(88)90106-X

[33] G. Rondeaux, M. Steven, and F. Baret, "Optimization of soil-adjusted vegetation indices," *Remote Sens Environ,* vol. 55, no. 2, pp. 95–107, 1996. Available: doi: 10.1016/0034-4257(95)00186-7

[34] A. J. Richardson and C. L. Wiegand, "Distinguishing vegetation from soil background information," *Photogramm Eng Remote Sensing,* vol. 43, no. 12, pp. 1541–1552, 1977.

[35] H. Xu, "Modification of normalised difference water index (NDWI) to enhance open water features in remotely sensed imagery," *Int J Remote Sens*, vol. 27, no. 14, pp. 3025–3033, 2006. Available: doi: 10.1080/01431160600589179

[36] Y. Zha, J. Gao, and S. Ni, "Use of normalized difference built-up index in automatically mapping urban areas from TM imagery," *Int J Remote Sens*, vol. 24, no. 3, pp. 583–594, 2003. Available: doi: 10.1080/01431160304987

[37] D. K. Hall, G. A. Riggs, and V. V Salomonson, "Development of methods for mapping global snow cover using moderate resolution imaging spectroradiometer data," *Remote Sens Environ,* vol. 54, no. 2, pp. 127–140, 1995. Available: doi: 10.1016/0034-4257(95)00137-P

[38] G. M. Foody, "Status of land cover classification accuracy assessment," *Remote Sens Environ,* vol. 80, no. 1, pp. 185–201, 2002, Available: doi: 10.1016/S0034-4257(01)00295-4.

[39] P. Olofsson, G. M. Foody, M. Herold, S. V Stehman, C. E. Woodcock, and M. A. Wulder, "Good practices for estimating area and assessing accuracy of land change," *Remote Sens Environ,* vol. 148, pp. 42–57, 2014, Available: doi: 10.1016/j.rse.2014.02.015.

[40] J. Liu et al., "Spatial patterns and driving forces of land use change in China during the early 21st century," *Journal of Geographical Sciences*, vol. 20, pp. 483–494, 2010. Available: doi: 10.1007/s11442-010-0483-4

[41] M. Kuhn, "Building predictive models in R using the caret package," *J Stat Softw,* vol. 28, pp. 1–26, 2008. Available: doi: 10.18637/jss.v028.i05

[42] W. Thuiller, B. Lafourcade, R. Engler, and M. B. Araújo, "BIOMOD–a platform for ensemble forecasting of species distributions," *Ecography,* vol. 32, no. 3, pp. 369–373, 2009. Available: doi: 10.1111/j.1600-0587.2008.05742.x

[43] P. O. Gislason, J. A. Benediktsson, and J. R. Sveinsson, "Random forests for land cover classification," *Pattern Recognit Lett,* vol. 27, no. 4, pp. 294–300, 2006. Available: doi: 10.1016/j.patrec.2005.08.011

[44] T. Chen and C. Guestrin, "Xgboost: A scalable tree boosting system," in Proceedings of the 22nd acm sigkdd international conference on knowledge discovery and data mining, 2016, pp. 785–794. Available: doi: 10.1145/2939672.2939785

[45] S. M. Lundberg and S.-I. Lee, "A unified approach to interpreting model predictions," *Adv Neural Inf Process Syst*, vol. 30, 2017.

[46] "Elevation-dependent warming in mountain regions of the world," *Nat Clim Chang,* vol. 5, no. 5, pp. 424–430, 2015. Available: doi: 10.1038/nclimate2563

[47] C. Wang, X. Zhang, and L. Liu, "Land Use Change in the Russian Far East and Its Driving Factors," *Land (Basel),* vol. 14, no. 4, p. 804, 2025. Available: doi: 10.3390/land14040804

[48] T. Bolch, et al., "Status and change of the cryosphere in the extended Hindu Kush Himalaya region," *The Hindu Kush Himalaya assessment: Mountains, climate change, sustainability and people,* pp. 209–255, 2019. Available: doi: 10.1007/978-3-319-92288-1_7

[49] G. X. He, et al., "Soil carbon, nitrogen and phosphorus stocks and ecological stoichiometry

characteristics of different vegetation restorations in degraded mountainous area of central Yunnan, China," *Acta Ecol. Sin,* vol. 40, pp. 4425–4435, 2020.

[50] R. Fensholt, et al., "Greenness in semi-arid areas across the globe 1981–2007—an Earth Observing Satellite based analysis of trends and drivers," *Remote Sens Environ,* vol. 121, pp. 144–158, 2012. Available: doi: 10.1016/j.rse.2012.01.017

[51] K. Li, Y. Zhang, Z. Zhang, and G. Lai, "A coarse-to-fine registration strategy for multi-sensor images with large resolution differences," *Remote Sens (Basel),* vol. 11, no. 4, p. 470, 2019. Available: doi: 10.3390/rs11040470

[52] J. Wang et al., "Land cover patterns in Mongolia and their spatiotemporal changes from 1990 to 2010," *Arabian Journal of Geosciences*, vol. 12, pp. 1–13, 2019. Available: doi: 10.1007/s12517-019-4893-z